JACS
JOURNAL OF THE AMERICAN CHEMICAL SOCIETY
Communication
pubs.acs.org/JACS

In Situ Imaging of Cu_2O under Reducing Conditions: Formation of Metallic Fronts by Mass Transfer

Ashleigh E. Baber,[†] Fang Xu,[†,§] Filip Dvorak,[∥] Kumudu Mudiyanselage,[†] Markus Soldemo,[⊥] Jonas Weissenrieder,[⊥] Sanjaya D. Senanayake,[†] Jerzy T. Sadowski,[‡] José A. Rodriguez,[†] Vladimír Matolín,[∥] Michael G. White,[†,§] and Darío J. Stacchiola*[,†]

[†]Chemistry Department and [‡]Center for Functional Nanomaterials, Brookhaven National Laboratory, Upton, New York 11973, United States

[§]Stony Brook University, Stony Brook, New York 11794, United States

[∥]Faculty of Mathematics and Physics, Charles University, Department of Surface and Plasma Science, Prague, Czech Republic

[⊥]KTH Royal Institute of Technology, Material Physics, Stockholm, Sweden

Supporting Information

ABSTRACT: Active catalytic sites have traditionally been analyzed based on static representations of surface structures and characterization of materials before or after reactions. We show here by a combination of *in situ* microscopy and spectroscopy techniques that, in the presence of reactants, an oxide catalyst's chemical state and morphology are dynamically modified. The reduction of Cu_2O films is studied under ambient pressures (AP) of CO. The use of complementary techniques allows us to identify intermediate surface oxide phases and determine how reaction fronts propagate across the surface by massive mass transfer of Cu atoms released during the reduction of the oxide phase in the presence of CO. High resolution *in situ* imaging by AP scanning tunneling microscopy (AP-STM) shows that the reduction of the oxide films is initiated at defects both on step edges and the center of oxide terraces.

Cu-based catalysts are used industrially for CO conversion reactions such as CO oxidation,[1,2] methanol synthesis,[3] and the water-gas shift.[4] CO oxidation is a prototypical reaction for heterogeneous catalysis,[5,6] and for CuO_x catalysts the rate of this reaction depends on the oxidation state of the substrate.[7] Model catalytic systems used to understand processes at the atomic level include supported Cu metal nanoparticles,[8−10] inverse catalysts (MO_x/Cu(111)[11,12]), and mixed oxides MO_x/Cu_2O.[13] Cu(111) oxidizes at 300 K,[14−16] forms a well-ordered Cu_2O(111) film at elevated temperatures[17−20] and can be further oxidized in the presence of a second oxide.[13] It has been proposed that CO reduces oxides via the Mars-van Krevelen mechanism and produces CO_2 using oxygen from the surface.[21,22] Certain surface species and catalyst phases are only stable in the presence of reactants, indicating a need for AP *in situ* characterization.[23,24] AP techniques have shown metals restructuring and alloys segregating under reactive gases, as well as catalyst oxidation state and chemical composition changes.[23,25−28] AP-STM images show an increase of the mobility of edge and kink atoms on metallic steps[28] and the lifting of the Pt(100)-hex reconstruction under CO,[29] as well as active oxygen species during ethylene epoxidation on Ag(111).[30] Atomic resolution of adsorbates has been demonstrated during reactions under vacuum conditions (10^{-8} mbar)[5] and via AP-STM,[31,32] but high resolution imaging of substrates under AP conditions has resulted in being more challenging.

Cu_2O/Cu(111) can be fully reduced with CO under UHV conditions at ∼800 K.[33] UHV-STM images taken as snapshots by quenching the reaction showed a transition from a long-range ordered oxide layer to a ring (glass-like) structure comprised of hexagons (hex), and pentagons and heptagons (5−7 structure) before fully reducing to the metallic Cu surface.[20,34] UHV-STM snapshots cannot however provide information about the origin and dynamic mechanism of the reduction. Here, we show *in situ* results from the CO reduction of a Cu_2O/Cu(111) model system with low energy electron microscopy (LEEM), ambient pressure scanning tunneling microscopy (AP-STM), AP infrared reflection absorption spectroscopy (IRRAS), and AP X-ray photoelectron spectroscopy (XPS). We report STM images showing highly resolved morphological, and therefore oxidation state, changes that occur during the reaction and identify the formation of a metallic phase front due to Cu mass transfer as the oxide film is reduced under ambient pressures of CO. The data presented contains the first resolved oxide surface imaged under AP reaction conditions, allowing us to monitor the reduction of the substrate *in situ*.

Long-range ordered Cu_2O(111)-like thin films grown on Cu(111) appear as rows.[17−20] Figure S.1A (see Supporting Information) shows a clean Cu(111) surface with large atomically flat terraces, with an atomic spacing of 0.256 nm, and a Cu_2O(111) film grown on Cu(111) (Figure S.1B), with a compressed hexagonal (row) structure having a 0.6 nm spacing.[17,20,34] Using LEEM, the reduction of the Cu_2O(111) film was monitored on a microscopic scale during CO exposure at 2×10^{-6} Torr and 575 K. Figure 1 shows a series of *in situ*, high temperature LEEM images progressing from the oxidized Cu_2O/Cu(111) to metallic Cu(111) recorded at 4 eV (see Movie 1 in Supporting Information). The inset in Figure 1A shows the μ-LEED pattern for Cu_2O/Cu(111) at 44 eV with its characteristic

Received: August 16, 2013
Published: October 29, 2013

dx.doi.org/10.1021/ja408506y | *J. Am. Chem. Soc.* 2013, 135, 16781−16784

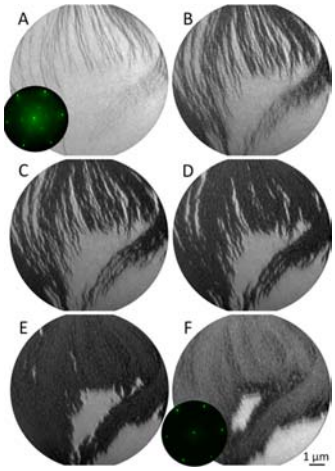

Figure 1. LEEM images recorded during the CO reduction of Cu_2O/Cu(111) at 575 K. (A) t = 454 s, inset shows a μ-LEED pattern of the Cu_2O(111) film; (B) t = 638 s; (C) t = 678 s; (D) t = 803 s; (E) t = 1013 s; (F) t = 1508 s, μ-LEED inset shows the hexagonal packing of metallic Cu.

double spots. During the CO exposure, the step edges (lines seen in Figure 1A) become darker as the reduction begins in high step density regions where terraces are narrow, and the metallic phase grows from the steps (Figure 1B through 1D). Figure 1E and 1F show that after CO has consumed the oxide in highly stepped areas, a front propagates across the surface in the center. After the reduction, μ-LEED (Figure 1F inset) shows a 1 × 1 diffraction pattern for metallic Cu(111). This microscopic view shows that metallic reaction fronts move across the surface as the oxide is reduced under vacuum conditions at elevated temperatures.

LEEM and μ-LEED highlight the dynamic global behavior, and STM can be used to show local changes in structure at the nanoscale. Figure 2 shows consecutive *in situ* AP-STM images of the reduction of Cu_2O/Cu(111) under 10 mTorr CO at 300 K in a region with two step edges (see Movie 2 in Supporting Information). Control experiments show no changes in the Cu(111) surface under similar conditions. CO molecules adsorbed to the STM tip help to enhance its sharpness.[35,36]

The reduction from the Cu_2O oxide rows to the hex/5−7 ring oxide, and then to metallic Cu is observed in the consecutive STM images in Figure 2, beginning with a fully oxidized surface in Figure 2A. After CO exposure for 281 s (Figure 2B), an area of metallic Cu is seen growing from the upper step edge. Metallic Cu areas are separated from the oxide row structures by bands of hex/5−7 rings. As CO consumes the oxygen from the oxide, loss of the long-range order is observed on the terraces of the Cu_2O(111) film (Figure 2C−G). The two step edges continually grow during the reduction, showing mass transfer of Cu atoms to the step edges during the reduction, resulting in a phase separation between the oxide and the metal. We propose that as Cu_2O is consumed by CO, the Cu atoms released from the oxide are highly mobile at 300 K in the presence of CO and rapidly diffuse, forming metallic Cu terraces.

The sintering of small metallic particles supported on metal substrates or oxide films has been shown previously by the mass transfer of atoms bonded to CO,[37−39] but metal/oxide phase separations as shown here have not been reported. The coverage of the three observed phases are plotted in Figure 2H, showing that the appearance of the intermediate ring structure precedes the metallic areas. The transition from the rows to the rings is

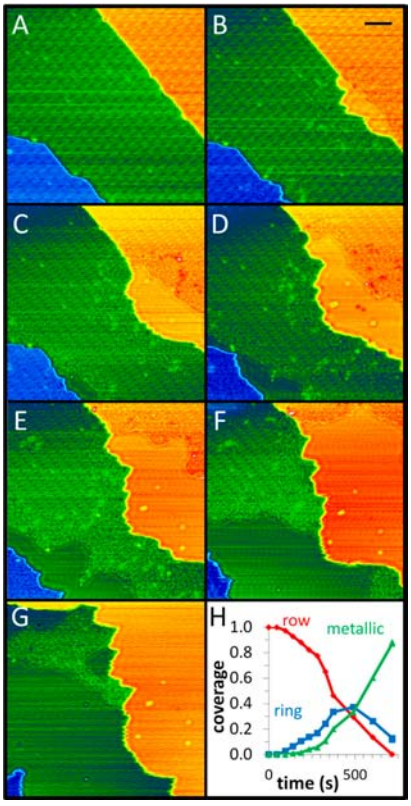

Figure 2. STM snapshots (see Movie 2) during the reduction of a Cu_2O film under 10 mTorr CO at 300 K after 46, 281, 374, 490, 603, 715, and 828 s (A−G); scale bar = 5 nm. (H) Phases coverages are plotted as a function of CO exposure. The color in the images corresponds to apparent height; scanning: 1.1 V, 0.83 nA.

slow, but after the ring structure appears, it quickly reduces to metallic Cu.

Consecutive AP-STM images are seen in Figure 3 (larger images in Figure S.5) on a Cu_2O/Cu(111) terrace during its reduction under 45 mTorr CO. The long-range order in Figure 3A is lost as the reduction progresses. A new intermediate structure was observed during the reduction of the Cu_2O(111) film, appearing as an ordered arrangement of bright protrusions in Figure 3C (see Figure S.2C in Supporting Information for the

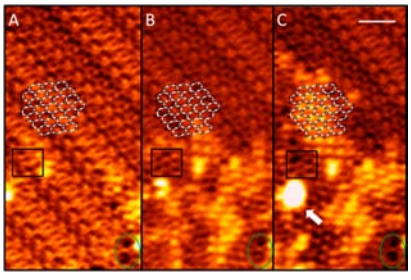

Figure 3. AP-STM images of the CO reduction (45 mTorr) of Cu_2O/Cu(111) at 300 K (green circle serves as landmark). (A) The Cu_2O(111)-"44" film has a compressed hexagonal O−Cu−O lattice. Schematic: O atoms are black, Cu atoms and chemisorbed O inside the hexagons are not shown. (B) The film buckles (bright protrusions) as it is reduced. (C) An arrangement of protrusions appears at the vertices of the hexagonal rings. The black square shows a ring oxide structure, and the arrow indicates the appearance of a Cu island. Scanning: 0.9 V, 0.78 nA, scale bar = 2 nm.

dx.doi.org/10.1021/ja408506y | *J. Am. Chem. Soc.* 2013, 135, 16781−16784

corresponding large scale image). The arrangement could be related to either (1) the adsorption of CO or (2) structural rearrangements of the $Cu_2O(111)$ film during its transformation to the ring structure. The reported height of CO on Cu(100) is 0.3 Å,[40] similar to the protrusions seen in Figure 3C. However, the residence time of the adsorbed CO on the $Cu_2O(111)$-"44" film at 300 K is expected to be short, and therefore highly unlikely to be imaged. Additionally, CO adsorbed on the hexagonal film would likely adopt a hexagonal packing rather than square. We therefore assign the ordered arrangement to changes in the structure of the $Cu_2O(111)$ film.

A square in Figure 3 shows a small area with hexagonal rings for comparison. The bright protrusions appeared in areas with rows, rather than on areas that had already converted to rings. A network of compressed Cu_2O hexagons (black circles are O atoms, Cu atoms are not shown), corresponding to the $Cu_2O(111)$-"44" film is superimposed on top of the three images to monitor the structural changes. Figure 3B and C show that the small bright protrusions in the ordered arrangement correspond with vertices of the Cu_2O hexagons. As CO begins to reduce the oxide at defects in the middle of a terrace, an apparent buckling of the oxide film away from the surface propagates, as the compressed hexagonal structure relaxes. The bright protrusions only appeared on the terrace oxide during reduction, and not at the step edges, which is buckling likely due to the constraint of the surrounding compressed hexagonal oxide. The appearance of small Cu islands is due to the mass transfer of Cu atoms released from the oxide during the reduction, as indicated by the arrow in Figure 3C (see also Figures S.2 and S.3). A large scale image of Figure 3 (see Figure S.2) and Figure 2 show that the released Cu is preferentially transferred to metallic fronts growing from step edges, in agreement with the LEEM data shown in Figure 1, but the nucleation and growth of Cu islands is also possible at defects far from steps.

IRRAS experiments show that CO adsorbed on Cu_2O/Cu(111) under UHV conditions at 120 K presents a peak at ~2097 cm^{-1}.[41] Similar to the adsorption of CO on Cu(111),[41] CO adsorbs weakly on Cu_2O/Cu(111) and desorbs molecularly at ~180 K, slightly higher than the ~160 K desorption temperature for CO on Cu(111).[41] Figure 4A shows the AP-IRRA spectra obtained by exposing Cu_2O/Cu(111) to CO; at 4.8 mTorr a weak IR peak appears at 2094 cm^{-1}, in addition to CO gas phase features (centered ~2143 cm^{-1}). The peak at 2094 cm^{-1} is assigned to CO adsorbed on the $Cu_2O(111)$ film.[41] The intensity of the IR peak at 2094 cm^{-1} increases as the CO pressure is increased to 10 mTorr. The pressure was then held for 10 min, and a series of IR spectra were collected. At 10 mTorr of CO, the intensity of the peak at 2094 cm^{-1} from adsorbed CO on the well-ordered oxide decreases with time until it disappears, corresponding to the reduction of the $Cu_2O(111)$ film. A very weak feature at ~2105 cm^{-1} is due to CO adsorbed on the hex/5−7 structure.[41] The weaker adsorption of CO on Cu(111) prevents its observation at 10 mTorr. After increasing the CO pressure to 80 and 266 mTorr only the peaks for adsorbed CO on Cu(111) at 2070 cm^{-1} and gas phase CO remain (bottom in Figure 4A). AP-IRRAS experiments confirm that CO adsorbs on the $Cu_2O(111)$ film and reduces it at 300 K under 10 mTorr.

Figure 4B shows O 1s spectra (photon energy = 750 eV) from AP-XPS as a function of time during the exposure of the Cu_2O/Cu(111) film to 10 mTorr CO at 300 K. The peak at ~530 eV, related to the oxide, decreases over time as CO reduces the Cu_2O. At time t = 0 s the sample is exposed to CO. No features were observed in the C 1s and O 1s regions related to the

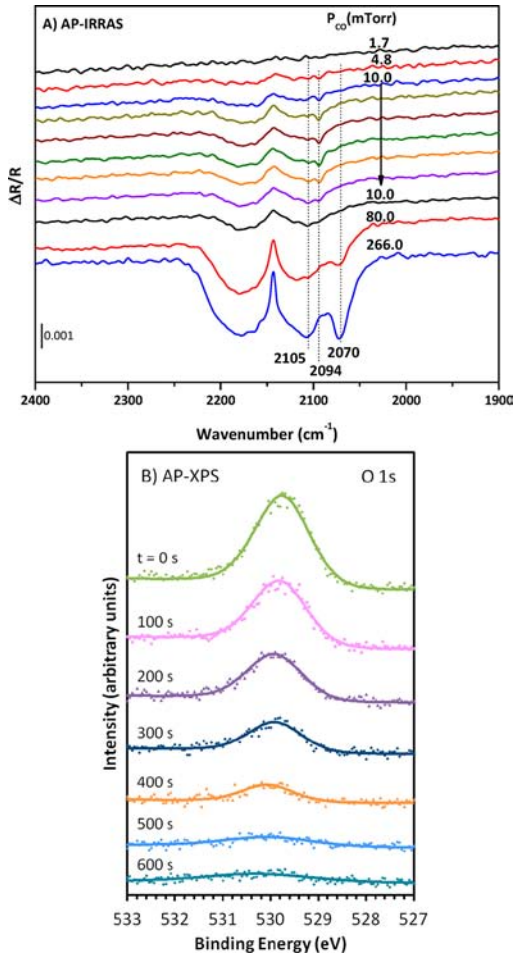

Figure 4. (A) IRRA spectra obtained during the exposure of Cu_2O/Cu(111) to CO. The pressure was held at 10 mTorr for 10 min and a series of IR spectra were collected, showing the reduction of the $Cu_2O(111)$ film. (B) AP-XPS O1s spectra during the 10 mTorr CO reduction of a $Cu_2O(111)$ film at 300 K.

formation of carbonaceous surface species such as carbonates, confirming that the only surface species during the reduction of Cu_2O is CO, as shown by IRRAS. The fast stage of the reduction process, seen in the AP-STM images as the metallic front propagates (5−7/hex to metallic), can be related to the AP-XPS spectra by:

$$A_{[\mathrm{XPS\ (O\ 1s)}]} = B_{[\mathrm{STM(row\ oxide)}]} = 1, \quad t = 0\ \mathrm{s}$$

$$A_{[\mathrm{XPS\ (O\ 1s)}]} = B_{[\mathrm{STM(row\ oxide)}]} + 0.67C_{[\mathrm{STM(ring\ oxide)}]}, \quad t > 0\ \mathrm{s}$$

$$B_{[\mathrm{STM(row\ oxide)}]} + C_{[\mathrm{STM(ring\ oxide)}]} + D_{(\mathrm{STM(metallic\ Cu)})} = 1$$

Before the reduction (t = 0 s), the O coverage is saturated and therefore the AP-XPS and AP-STM areas can be normalized to 1. After the reaction starts (t > 0 s) the $Cu_2O(111)$ film converts to the ring oxide, eliminating O from the center of the compressed hexagons. The lower O coverage is accounted for by a normalization factor of 0.67 for the ring oxide structure. Upon comparing the slope of the disappearance of oxide structures as a function of time for AP-XPS and AP-STM measurements during the fast reaction regime, under 10 mTorr of CO and 300 K, we find a rate of disappearance of oxygen of $(2.1 \pm 0.1) \times 10^{-3}\ s^{-1}$ for our AP-XPS results and $(1.8 \pm 0.1) \times 10^{-3}\ s^{-1}$ from AP-STM.

The reduction of a Cu_2O/Cu(111) film by CO was studied *in situ*. LEEM imaging shows the propagation of metallic fronts as

dx.doi.org/10.1021/ja408506y | J. Am. Chem. Soc. 2013, 135, 16781−16784

the reduction progresses. AP-XPS and AP-IRRAS show that the reduction of Cu_2O proceeds in the presence of only adsorbed CO molecules. Using AP-STM, the reaction was monitored at the nanoscale, observing the structural transformation from the $Cu_2O(111)$ film to glass-like hex/5−7 ring structures, to metallic Cu. The hex/5−7 intermediate propagated across the surface as a front and precursor to the metallic phase. *In situ* measurements show that the reduction begins at defects in the $Cu_2O(111)$ film terraces and step edges. At terrace defects, the oxide buckles during reduction, appearing as bright protrusions before converting into the ring structure. Most of the Cu atoms released by reduction of Cu_2O in the presence of CO undergo mass transfer to step edges, causing a massive reconstruction and phase separation between the oxide and metal. The AP *in situ* experiments presented here show the dynamic nature of catalytic surfaces, including oxidation state changes and morphological restructuring. Unprecedented highly resolved images under ambient pressures allow us a unique look into the dynamic nature of active sites generated in the presence of the reactants. This visualization challenges the traditional static view of catalysts and will help to promote the generation of a new framework for the interpretation of catalysis at the molecular level.

■ ASSOCIATED CONTENT

Supporting Information

Two movies, experimental methods, and further details are included in the Supporting Information. This material is available free of charge via the Internet at http://pubs.acs.org.

■ AUTHOR INFORMATION

Corresponding Author

djs@bnl.gov

Notes

The authors declare no competing financial interest.

■ ACKNOWLEDGMENTS

The work at Brookhaven National Laboratory was carried out under Contract No. DE-AC02-98CH10886 with the U.S. Department of Energy, Office of Science, and supported by its Division of Chemical Sciences, Geosciences, and Biosciences within the Office of Basic Energy Sciences. We are thankful to the Swedish Research Council (VR) for financial support. Jan Knudsen, Joachim Schnadt, and the Max-lab staff are acknowledged for their support. F.D. and V.M. thank the Ministry of Education of the Czech Republic for financial support under Project LH11017.

■ REFERENCES

(1) Szanyi, J.; Goodman, D. W. *Catal. Lett.* **1993**, *21*, 165.
(2) Domagala, M. E.; Campbell, C. T. *Catal. Lett.* **1991**, *9*, 65.
(3) Klier, K. Methanol Synthesis. In *Advances in Catalysis*; Eley, D. D., Pines, H., Weisz, P. B., Eds.; Academic Press: 1982; Vol. *31*; pp 243
(4) Newsome, D. S. *Catal. Rev.* **1980**, *21*, 275.
(5) Wintterlin, J.; Völkening, S.; Janssens, T. V. W.; Zambelli, T.; Ertl, G. *Science* **1997**, *278*, 1931.
(6) Freund, H.-J.; Meijer, G.; Scheffler, M.; Schlögl, R.; Wolf, M. *Angew. Chem., Int. Ed.* **2011**, *50*, 10064.
(7) Jernigan, G. G.; Somorjai, G. A. *J. Catal.* **1994**, *147*, 567.
(8) Shishido, T.; Yamamoto, M.; Li, D.; Tian, Y.; Morioka, H.; Honda, M.; Sano, T.; Takehira, K. *Appl. Catal., A* **2006**, *303*, 62.
(9) Behrens, M.; Studt, F.; Kasatkin, I.; Kühl, S.; Hävecker, M.; Abild-Pedersen, F.; Zander, S.; Girgsdies, F.; Kurr, P.; Kniep, B.-L.; Tovar, M.; Fischer, R. W.; Nørskov, J. K.; Schlögl, R. *Science* **2012**, *336*, 893.
(10) Park, J. B.; Graciani, J.; Evans, J.; Stacchiola, D.; Senanayake, S. D.; Barrio, L.; Liu, P.; Sanz, J. F.; Hrbek, J.; Rodriguez, J. A. *J. Am. Chem. Soc.* **2010**, *132*, 356.
(11) Mudiyanselage, K.; Senanayake, S. D.; Feria, L.; Kundu, S.; Baber, A. E.; Graciani, J.; Vidal, A. B.; Agnoli, S.; Evans, J.; Chang, R.; Axnanda, S.; Liu, Z.; Sanz, J. F.; Liu, P.; Rodriguez, J. A.; Stacchiola, D. J. *Angew. Chem., Int. Ed.* **2013**, *52*, 5101.
(12) Rodriguez, J. A.; Graciani, J.; Evans, J.; Park, J. B.; Yang, F.; Stacchiola, D.; Senanayake, S. D.; Ma, S. G.; Perez, M.; Liu, P.; Sanz, J. F.; Hrbek, J. *Angew. Chem., Int. Ed.* **2009**, *48*, 8047.
(13) Yang, F.; Choi, Y.; Agnoli, S.; Liu, P.; Stacchiola, D.; Hrbek, J.; Rodriguez, J. A. *J. Phys. Chem. C* **2011**, *115*, 23062.
(14) Lawton, T. J.; Pushkarev, V.; Broitman, E.; Reinicker, A.; Sykes, E. C. H.; Gellman, A. J. *J. Phys. Chem. C* **2012**, *116*, 16054.
(15) Wiame, F.; Maurice, V.; Marcus, P. *Surf. Sci.* **2007**, *601*, 1193.
(16) Dubois, L. H. *Surf. Sci.* **1982**, *119*, 399.
(17) Jensen, F.; Besenbacher, F.; Lægsgaard, E.; Stensgaard, I. *Surf. Sci. Lett.* **1991**, *259*, L774.
(18) Jensen, F.; Besenbacher, F.; Stensgaard, I. *Surf. Sci.* **1992**, *269*−*270*, 400.
(19) Matsumoto, T.; Bennett, R. A.; Stone, P.; Yamada, T.; Domen, K.; Bowker, M. *Surf. Sci.* **2001**, *471*, 225.
(20) Yang, F.; Choi, Y. M.; Liu, P.; Hrbek, J.; Rodriguez, J. A. *J. Phys. Chem. C.* **2010**, *114*, 17042.
(21) Mars, P.; van Krevelen, D. W. *Chem. Eng. Sci.* **1954**, *3*, 41.
(22) Lundgren, E.; Gustafson, J.; Resta, A.; Weissenrieder, J.; Mikkelsen, A.; Andersen, J. N.; Köhler, L.; Kresse, G.; Klikovits, J.; Biederman, A.; Schmid, M.; Varga, P. *J. Electron Spectrosc.* **2005**, *144*−*147*, 367.
(23) Tao, F.; Salmeron, M. *Science* **2011**, *331*, 171.
(24) Zhang, S.; Nguyen, L.; Zhu, Y.; Zhan, S.; Tsung, C.-K.; Tao, F. *Acc. Chem. Res.* **2013**, *46*, 1731.
(25) Tao, F.; Zhang, S.; Nguyen, L.; Zhang, X. *Chem. Soc. Rev.* **2012**, *41*, 7980.
(26) Zafeiratos, S.; Piccinin, S.; Teschner, D. *Catal. Sci. Technol.* **2012**, *2*, 1787.
(27) Salmeron, M.; Schlögl, R. *Surf. Sci. Rep.* **2008**, *63*, 169.
(28) Nguyen, L.; Cheng, F.; Zhang, S.; Tao, F. *J. Phys. Chem. C* **2012**, *117*, 971.
(29) Zhu, Z.; Butcher, D. R.; Mao, B.; Liu, Z.; Salmeron, M.; Somorjai, G. A. *J. Phys. Chem. C* **2013**, *117*, 2799.
(30) Böcklein, S.; Günther, S.; Wintterlin, J. *Angew. Chem., Int. Ed.* **2013**, *52*, 5518.
(31) Laegsgaard, E.; Osterlund, L.; Thostrup, P.; Rasmussen, P. B.; Stensgaard, I.; Besenbacher, F. *Rev. Sci. Instrum.* **2001**, *72*, 3537.
(32) Reichelt, R.; Gunther, S.; Ro; Wintterlin, J.; Kubias, B.; Jakobi, B.; Schlogl, R. *Phys. Chem. Chem. Phys.* **2007**, *9*, 3590.
(33) Yang, F.; Choi, Y.; Liu, P.; Hrbek, J.; Rodriguez, J. A. *J. Phys. Chem. C* **2010**, *114*, 17042.
(34) Yang, F.; Choi, Y.; Liu, P.; Stacchiola, D.; Hrbek, J.; Rodriguez, J. A. *J. Am. Chem. Soc.* **2011**, *133*, 11474.
(35) Bartels, L.; Meyer, G.; Rieder, K. H. *Appl. Phys. Lett.* **1997**, *71*, 213.
(36) Hahn, J. R.; Lee, H. J.; Ho, W. *Phys. Rev. Lett.* **2000**, *85*, 1914.
(37) Hrbek, J.; Hoffmann, F. M.; Park, J. B.; Liu, P.; Stacchiola, D.; Hoo, Y. S.; Ma, S.; Nambu, A.; Rodriguez, J. A.; White, M. G. *J. Am. Chem. Soc.* **2008**, *130*, 17272.
(38) Lu, J. L.; Kaya, S.; Weissenrieder, J.; Gao, H. J.; Shaikhutdinov, S.; Freund, H. J. *Surf. Sci.* **2006**, *600*, L153.
(39) Starr, D.; Shaikhutdinov, S.; Freund, H.-J. *Top. Catal.* **2005**, *36*, 33.
(40) Thamankar, R.; Meyerheim, H. L.; Ernst, A.; Ostanin, S.; Maznichenko, I. V.; Soyka, E.; Mertig, I.; Kirschner, J. *Phys. Rev. Lett.* **2011**, *106*, 106101.
(41) Mudiyanselage, K.; An, W.; Yang, F.; Liu, P.; Stacchiola, D. J. *Phys. Chem. Chem. Phys.* **2013**, *15*, 10726.